Master's Thesis of Science

Structural basis of membrane protein stabilization by nanodisc

나노디스크의 막단백질 안정화 기작에 대한 구조적 연구

February 2023

Graduate School of Natural Sciences
Seoul National University
Biological Sciences Major

So-Jung Kim

Structural basis of membrane protein stabilization by nanodisc

Advisor: Professor Soung-Hun Roh, Ph. D.

Submitting a master's thesis in science

February 2023

Graduate School of Natural Sciences
Seoul National University
Biological Sciences Major

So-Jung Kim

Confirming the master's thesis written by
So-Jung Kim
February 2023

Chair _____(Seal)

Vice Chair _____(Seal)

Examiner _____(Seal)

ABSTRACT

Structural basis of membrane protein stabilization by nanodisc

So-Jung Kim

School of Biological Sciences

The Graduate School

Seoul National University

While the nanodisc is being utilized in recent structural studies of membrane proteins, its stabilizing mechanisms on these proteins are still unknown. Here, we comprehensively analyzed the molecular distribution of various membrane proteins within the nanodiscs using a quantitative model of 3D variability results gathered from nine separate cryo-EM EMPIAR datasets. Our analysis revealed that the membrane proteins embedded in nanodiscs mostly migrate to the edge of the nanodisc to make proximal contacts to the membrane scaffold protein. Notably, the transmembrane helices of E. coli cytochrome bd-I oxidase clearly display a direct interaction

with the MSP. Through the B-factor analysis of the V-ATPase structure, we also observed that the stabilization of membrane protein is induced by the direct interaction with the MSP. Finally, we noticed an improvement in the local resolution of the protein density near the interaction site with the MSP, although the difference in overall resolution was not significant. Collectively, our study proposes that the membrane protein inside the nanodisc is stabilized by direct interaction with the MSP.

Keyword : Nanodisc, Membrane Scaffold Protein(MSP), Membrane protein, Cryo-EM

Student Number : 2020-24930

CONTENTS

LISTS OF FIGURES

Chapter 1

Introduction

1.1. Background

1.1.1. Study of membrane proteins and membrane mimetic technology

Membrane proteins (MPs) play an important role in numerous biological phenomena such as transport, enzyme activity, and signal transduction. Problems with MPs have been associated with ailments such as Parkinson's, Alzheimer's, atherosclerosis and cystic fibrosis[1]. As such, these proteins play a crucial role as pharmaceutical targets. Clarifying their 3D structure will play a key role for understanding the function and for studying structural-based drug discovery. The major bottleneck constraining the structural determination of MPs arises from the purification process due to issues such as aggregation, loss of function, and difficulty in crystallization. These limitations are being overcome with the recent development of cryo-EM and various MP reconstitution methods. The two most representative reconstitution methods for MPs are through the use of detergent and nanodiscs[2]. Structural determination of MPs is mostly done using samples in detergent, but there are concerns that the detergent environment is different from the native bilayer environment for the MP and thus may affect its functional conformation and overall stability. For this reason, reconstitution in nanodisc has been popularized recently since it provides a native-like environment with the lipid bilayer.[3] Furthermore, reports are suggesting that reconstitution in nanodisc yields a higher resolution structure through cryo-EM. Examples

include structures of TRPV1[4] and NompC[5] (Fig. 1). This literature attributes the improvement of resolution to the nanodisc environment, but there are still too many variables such as buffers used, microscope quality, imaging condition, and processing method that make it difficult to support the validity of such claims.

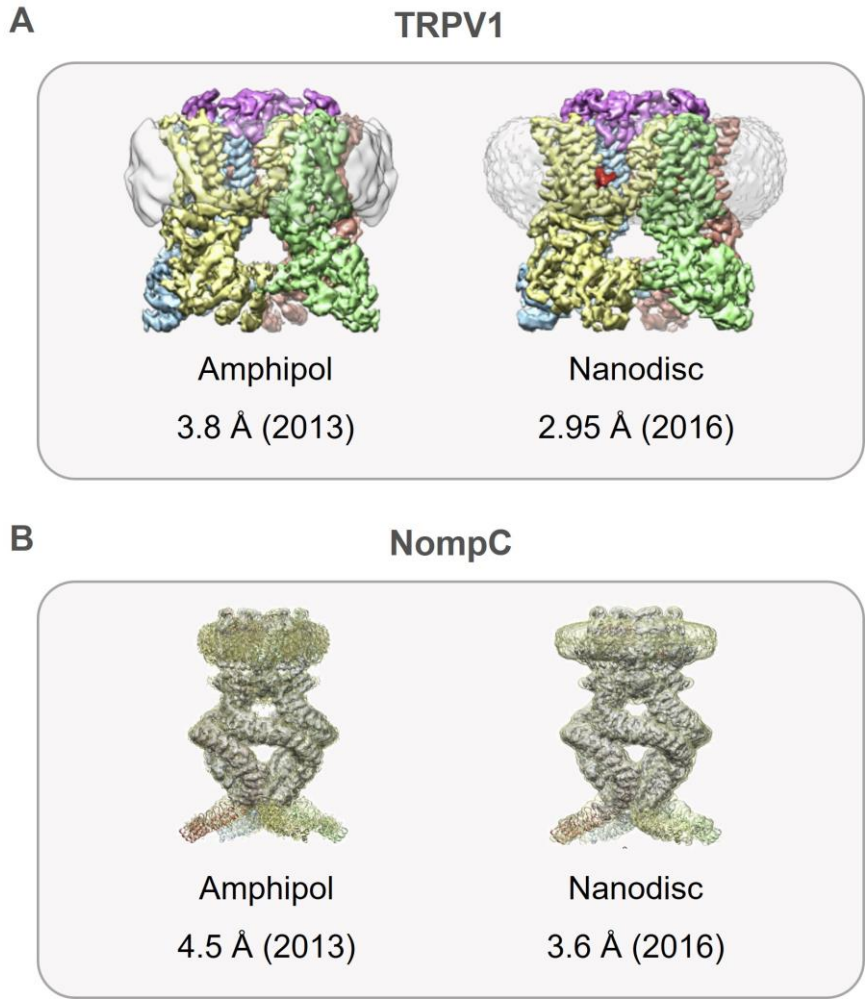

Figure 1. TRPV1 and NompC in amphipol and nanodisc

(A) TRPV1 reconstituted in amphipol and nanodisc.[4] EM densities for amphipol and nanodisc are shown in gray. Amphipol-reconstituted (3.8 Å) and nanodisc-reconstituted (2.95 Å) structures are shown. (B) 3D reconstruction of NompC in amphipol (4.5 Å) and nanodisc (3.6 Å).[5] Both proteins exhibit improved resolution when reconstituted in nanodisc

1.1.2. Origin and characteristic features of nanodisc

The lipid bilayer of the nanodisc embeds the hydrophobic transmembrane (TM) region of the MP, and the membrane scaffold protein (MSP), an amphipathic helical protein, envelops to stabilize the whole structure.[6] The structure of nanodisc originates from the HDL surrounded by apolipoprotein A-1; engineered apolipoprotein A-1 is used as the MSP to confer a stable structure of the nanodisc (Fig. 2). The formation of nanodisc occurs via self-assembly whereby a mono-dispersed discoidal form is created depending on the size of the MSP. Depending on the size of the MP, various MSPs can be engineered to accommodate the diameter of the overall nanodisc (Fig. 3).[7] As the MSP bilayer is stabilized with the formation of nanodisc, numerous salt bridges are created. These interactions are prone to alter,[8] however, and thus a high-resolution structure of the MSP strands is difficult to observe in datasets (Fig. 4). Studies of nanodisc properties are mainly done using the empty nanodiscs. Due to the structural fluidity of the nanodisc, MD simulation was used primarily to observe their properties.[9] According to a recent study, MPs can be stabilized at the edge of the nanodisc near the MSP rather than staying primarily in the center of the nanodisc fully embedded within the lipid bilayer as previously expected (Fig. 5). However, the MP used in this simulation is functionally involved with the rearrangement of the lipid bilayer to signal apoptosis in cells.[10] Because of this, we require further research to generalize the effect observed in their

MD simulation.

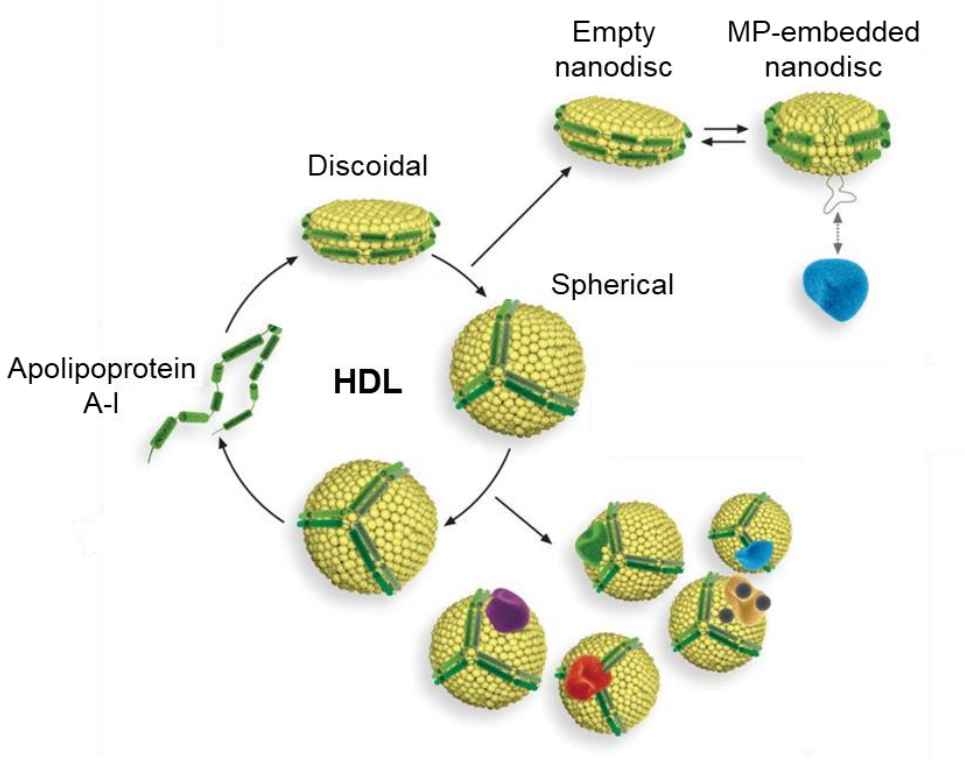

Figure 2. HDL particle complexity and application to nanodisc

Normal HDL metabolism affects the modulation of the composition and structure of lipoprotein.[11] HDL adopts either a discoidal or spherical shape based on the amount of lipid enrichment. In either case, Apolipoprotein A-I envelops the nanodisc. For nanodisc reconstitution of MPs, engineered Apolipoprotein A-I is used to create membrane scaffold protein (MSP).

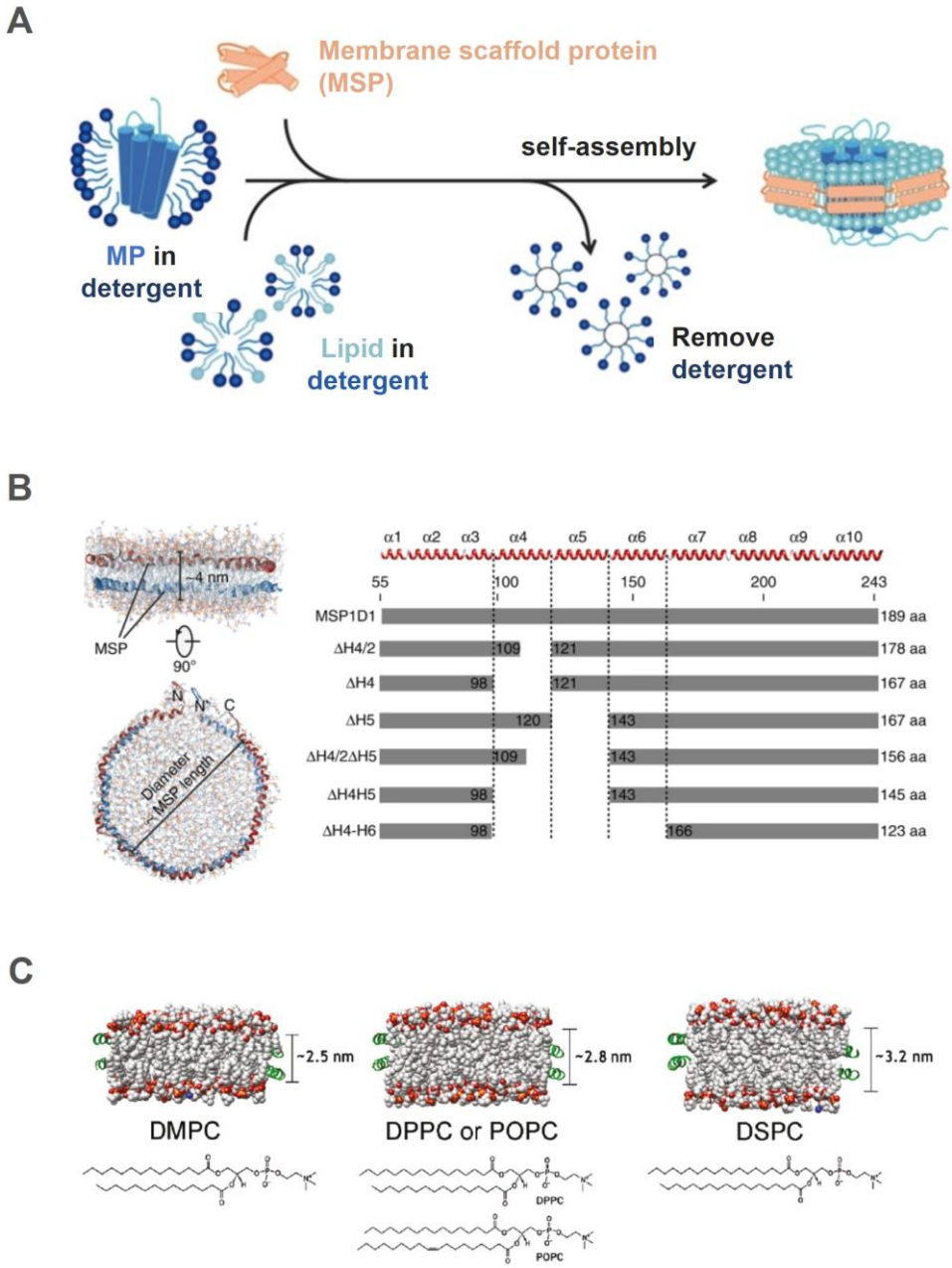

Figure 3. Nanodisc self-assembly and influencing factors

(A) Schematic diagram of the nanodisc self-assembly protocol.[12] Detergent-solubilized MP is incubated with MSP and lipid-detergent micelle. Nanodisc self-assembly initializes after the detergent is removed.

(B) Structural model of nanodisc and various MSP constructs. The diameter of the nanodisc is determined according to the length of the MSP.[13] (C) Depiction of the approximate thickness of nanodisc as determined according to the types of lipid used.[14]

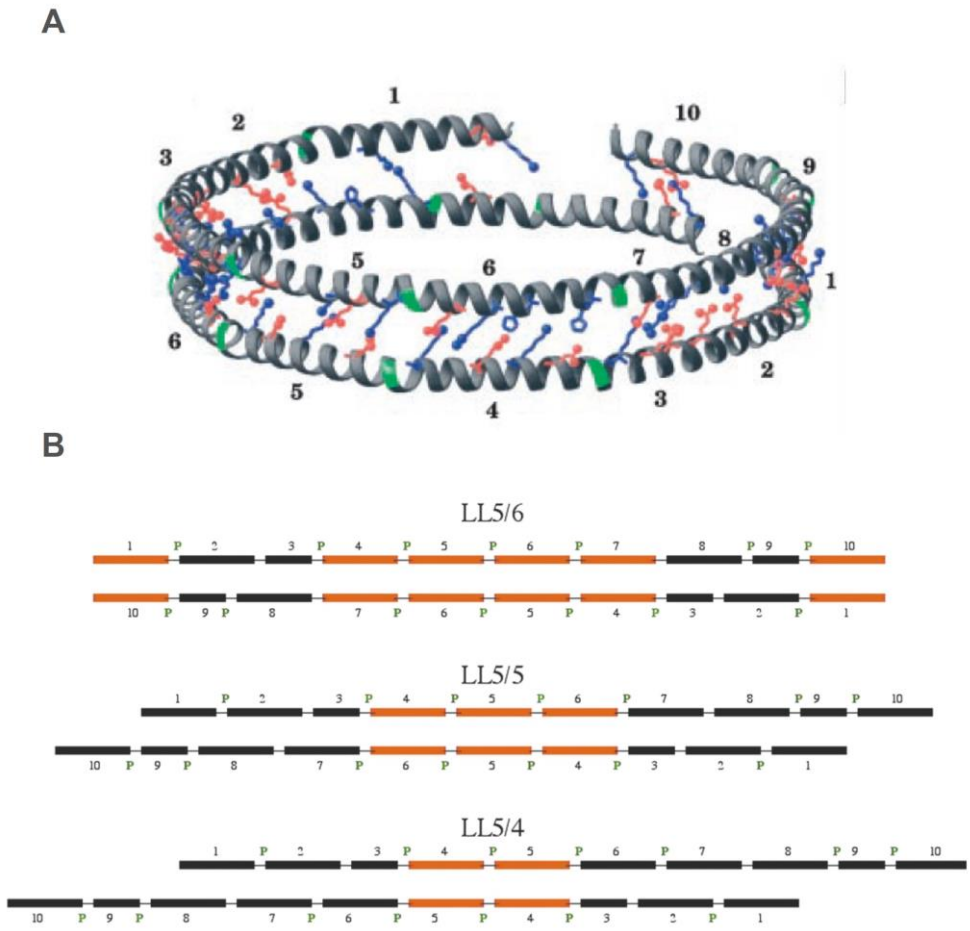

Figure 4. Structure and interhelical salt bridges of the MSP

(A) Ribbon model of MSP bilayer. Helix numbers are labeled. Residues involved in the MSP−MSP salt bridges are indicated. Basic residues are marked in blue, acidic residues in red, and prolines in green.[15] (B) A schematic diagram showing the alignment of two MSPs. Helices that are juxtaposed in alignment are colored in orange.[8]

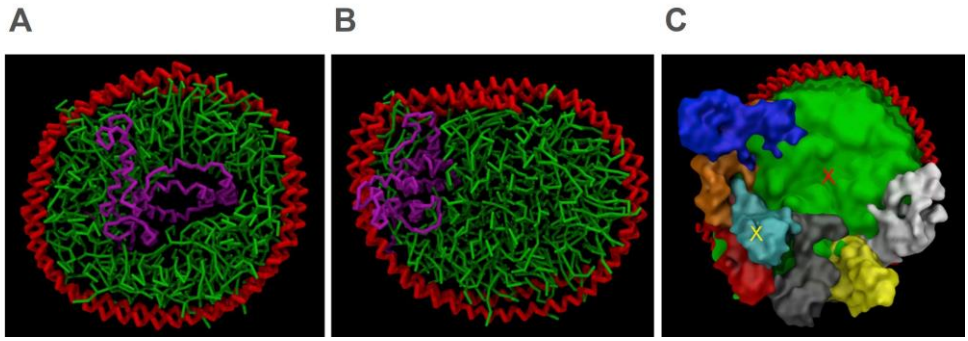

Figure 5. MD simulation of nanodisc with membrane protein

(A) Initial configuration of MP (purple) embedded in nanodisc for MD simulation. The MSP is shown as a red helix and lipid molecules are depicted in green. (B) Equilibrated configuration of MP embedded nanodisc. (C) 20 different simulations are run, and MP was found in seven potential places. Red X marks the initial position, while yellow X marks the N-C termini of the MSP.[10]

1.2. Purpose of this study

1.2.1. Limitation of previous research

Although the use of nanodisc for the purification of MP has increased in recent years due to the native-like lipidic environment it provides, we still lack a comprehensive study of the properties of nanodiscs, especially with the MPs embedded inside. This is mainly because nanodisc exhibits large structural fluidity and therefore it is difficult to obtain a high-resolution structure of nanodisc. Furthermore, focused classification and processing are done on the MP itself rather than the nanodisc in most existing datasets, proving the analysis of the effect of nanodisc on the MP even more difficult. At this stage, there is a deficiency in the study of the effect of nanodisc on the MP to provide a general explanation. As more structures of MPs embedded in nanodiscs are being published, we need research to explore a generalized effect of nanodisc on the MP and vice-versa.

1.2.2. Significance and application

To elucidate the effect of the MSP on the MP in nanodisc, it is prudent to study the MP-embedded nanodisc. To generalize the effect of nanodisc on MPs, it is useful to look at various MPs embedded in nanodiscs. Based on this understanding, if we could delineate the advantages of using nanodiscs rather than detergent, amphipol or other purification environments, we maybe able to

suggest nanodisc reconstruction as a generally more effective purification method. Furthermore, the knowledge of the interaction between nanodisc and target MP could aid us during the 3D reconstruction processing step.

Chapter 2

Materials and Methods

2.1. Reconstruction 3D structures of a membrane protein embedded nanodisc

All data were either obtained from the EMPIAR (https://www.ebi.ac.uk/empiar/) and downloaded from the least processed file type on the list (movie-micrograph-particle) or received personally V_0 complex. All data were imported to CryoSPARC[16]. The input values of each data are shown in Table 1.

We used MotionCor2[17] to perform motion correction after importing the movie files. CTF estimation was carried out using CTFFIND4[18], and the micrograph imported was carried out at this stage. After that, 2D templates were created by using a blob picker, and the second round of particle picking was carried out using template-based picking. Based on the 2D reference obtained, the initial 3D model was built with C1 symmetry. In the case of imported particles, the 2D classification was performed to select for viable particles, and the initial 3D model was created in the same way using the 2D templates. Based on the initial model created, the map was refined by repeating Non-uniform (NU) refinement and Heterogenous refinement. Once the resolution reached the published number, we carried out global and local CTF refinement. Then we performed another round of non-uniform refinement of the particles after CTF refinement.

Protein			EMPIAR EMDB PDB	Published Resolution (Å)	Reprocessing resolution (Å)	MSP	Lipid	MP : MSP : Lipid
TRP family	TRPV1		10059 8117 5IRX	2.95	2.79	MSP 2N2	Soybean PC	1 : 1 : 150 ~ 1 : 1.5 : 225
	TRPV 5	1-660	10255 0593 6O1N	2.9	2.88	MSP 2N2	Soy PC	1 : 2.5 : 100
		W583A	10253 0605 6O1U	2.85	2.85	MSP 2N2	Soy PC	1 : 1.5 : 150
	TRPM4		10127 7133 6BQV	3.1	2.86	MSP 2N2	Soy PC	1 : 3 : 390
TMEM16 family	TMEM16A		10123 7095 6BGI	3.8	3.48	MSP 2N2	Soy PC	1 : 4 : 100
	TMEM16F		10280 20246 6P48	3.3	3.06	MSP 2N2	SoyPC : POPC : POPE : POPS = 6 : 3 : 3 : 1	1 : 4 : 100
	afTMEM16		10240 8959 6E1O	3.59	3.83	MSP 1E3	POPE : POPG = 3 : 1	1 : 2.5 : 250
Anion channel	LRRC8A		10258 0562 6NZW	3.21	3.09	MSP1 E3D1	POPC	1 : 2.5 : 250
Hemichannel	Innexin6		10291 9973 6KFH	3.6	3.37	MSP 2N2	POPC	1 : 0.5 : 30
Cytochrome bd-I oxidase			- 4908 6RKO	2.68	-	MSP 1D1	POPC	1 : 10 : 400
V-ATPase V_0 complex			- 30035 6M0R	2.7	2.82	MSP1 E3D1	*E.coli* total lipid extract	1 : 50 : 1250
AftD			10399 21580 6W98	2.9	2.98	MSP1 E3D1	*E.coli* total lipid extract	1 : 6 : 360
Alg6			- 10258 6SNI	3.0	-	MSP 1D1	Yeast polar lipid extract	1 : 6 : 390

Table 1. Datasets utilized from outside sources

2.2. Analysis of nanodisc heterogeneity

For nanodisc structural heterogeneity analysis, we first use UCSF Chimera[19] to create a map corresponding to the nanodisc based on the final map. After aligning the final map in CryoSPARC and PDB file, we used the color zone value of 5 to distinguish between protein and nanodisc. Then, we used a segment map to erase the map of the nanodisc region thoroughly that overlaps with the protein. After isolating the nanodisc, we give the maximum value of the gaussian volume filter to erase the map details. The nanodisc map is imported back into CryoSPARC and then we created a mask of the nanodisc region using a volume tool. The type of output volume was given as a mask and dilation radius and soft padding width of 3.

After the final processing, the particles proceeded with the symmetry expansion by each symmetry. Then we added the output of this work and the map of the nanodisc that was created previously as the input value for 3D Variability Analysis (3DVA)[20]. The filter resolution value of 3DVA was 7, and the number of modes to solve was 3. Afterward, the output mode was intermediate in 3D variability display, and the 3D variability display output was checked using Chimera.

For quantitative analysis of heterogeneity in protein-embedded nanodisc, we divided the output mode cluster into 20 frames in the 3D variability display. To quantify the relative location of the MP relative to the MSP within the nanodisc as well as the

varying changes in the shape of the nanodisc itself, we considered five different variables for our study (Fig. 6A). For the nanodisc itself, we assumed it adopts an elliptical shape in 2D projection. We were able to consider only the 2D projection rather than the entire 3D as the shape of the nanodisc isn't an ellipsoid in 3D but rather an elliptical cylinder with the upper and lower part of the nanodisc more or less flat. The variables considered for the nanodisc include: the radius of the long axis of the ellipse denoted "a," the radius of the short axis of the ellipse denoted "b," and the focal point of the nanodisc C mathematically described by $C = \sqrt{a^2 - b^2}$. Varying values of the focal point C describe the changes in the shape of the elliptical shape of the nanodisc itself.

As for the variables describing the position of the MP within the nanodisc relative to the MSP, we considered the angle "Θ" formed between the long axis "a" and the line connecting the center of the nanodisc to the center of the MP. The length of the line connecting the centers of the nanodisc and the MP was described by the variable "R."

We analyzed three orthogonal yet complete "modes" resulting from the 3DVA. For each mode, the motion of the MP relative to the nanodisc was such that all but one variable was fixed. For each case, we normalized the maximum value at 10 and binned by five intervals. The homogeneous distribution graph was calculated differently for each variable. For instance, for modes where R is allowed to vary but other variables such as Θ and C are

fixed, the cross-section of the nanodisc forms either a fixed circle or an ellipse depending on the given C value. For C=0, any frames of the 3DVA with the same R-value are degenerate as they are indistinguishable from one another. In this case, the homogeneous distribution graph was calculated by adding the degeneracies together within the range of normalization with Nr referring to normalized value of R (for 0< nR <2, 1/25 of total particles, for 2 < nR < 4, 3/25 of total particles, for 4 < nR < 6, 5/25 of total particles, for 6 < nR < 8, 7/25 of total particles, and for 8 < nR < 10, 9/25 total particles) (Fig. 6B). When C is taken as the variable with normalization done with C (nC), even if the nR value is the same each frame is uniquely defined with varying C value. Thus, the homogeneous distribution graph for this case is a uniform distribution graph (Fig. 6C).

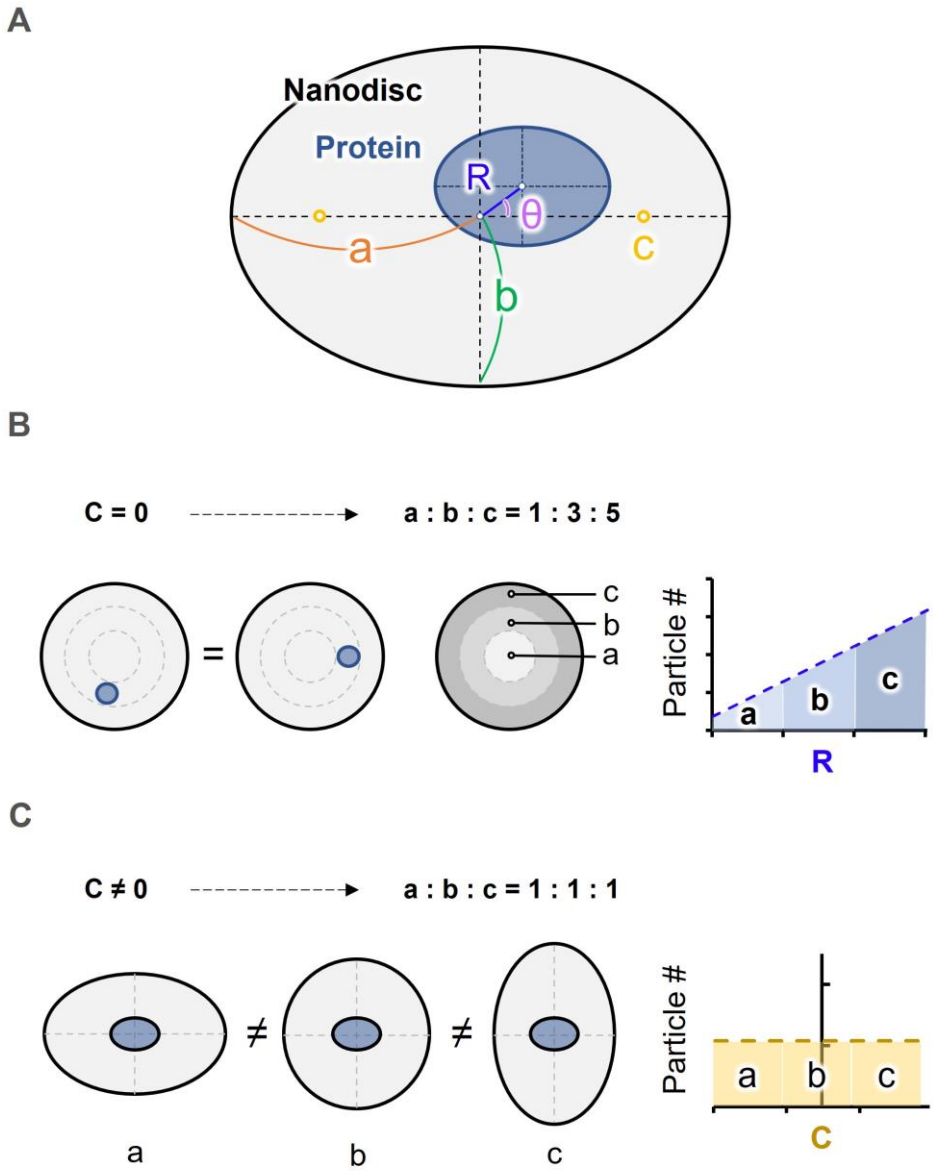

Figure 6. Schematic of the quantitative model used to analyze the distribution of membrane protein within the nanodisc

(A) MP embedded nanodisc model with variables. 'a' is the radius of the long axis of the ellipse. 'b' is the radius of the short axis of the ellipse. 'R' is the distance between the center of the nanodisc and the center of the MP. 'C' is the focal point value of the nanodisc (degree of deformation of

the nanodisc). The angle 'θ' formed between the long axis 'a' and the line connecting the center of the nanodisc to the center of the MP. (B) Calculating homogeneous distribution graph for variable 'R'. The area with the same R-value in nanodisc is indicated as a, b and c. The graph shows some particles that can be distributed in the corresponding parts. The larger the R-value, the more particles can be distributed. (C) Calculating homogeneous distribution graph for variable 'C' Nanodisc with different C values are indicated as a, b and c. The graph shows the number of particles that can be distributed in the corresponding parts. Regardless of C values, the particle has an even distribution.

2.3. Surface charge mapping on membrane protein and marking MSP structure

We displayed published structural maps of various MP using the Coulombic surface coloring feature in Chimera to highlight the surface charges. Then we applied a 3 Å low-pass filter to the nanodisc density as well as the MP in CryoSPARC. Then in Chimera, we separated only the density of the MSP from the filtered map through a segmentation process.

2.4. High-resolution MSP sequence candidates search

We isolated only the EM density corresponding to the MSP from a 3 Å low-pass filtered map of the cytochrome bd-I oxidase protein using the same process as described above. From here, the map was resegmented to allow the observation of the side-chain density map of the MSP. The candidate sequence came from the full sequences of MSP1D1 used in the nanodisc reconstitution of cytochrome bd-I oxidase (Fig. 7A). The high-resolution MSP map is composed of an eight-turn α-helix. Considering 3.6 amino acids per turn of α-helix, we estimate the total length as 29 amino acids. To determine the candidate sequences within the MSP, we used the 3^{rd}, 10^{th}, and 18^{th} bulky amino acids from the MP contact side as a reference within the high-resolution MSP map (Fig. 7B). For the

fitting, the 3rd residue in the chain was chosen to be either F, K, Y, or R as the bulkiest side chains. This leaves 30 candidate sequences of MSP that may fit into the MSP map. The 10th and 18th residues also showed bulky side chain densities, which allowed us to eliminate residues A, P, G, and V occupying those sites. Through this further process of elimination, we were left with seven final candidate sequences (Fig. 7C).

2.5. MSP model fitting and validation

Initial model fitting for all seven candidate sequences of MSP was done using ISOLDE[21], an MD simulation-based software. We used the default setting values for all parameters except for α-helix restrain. Then using the real-space refinement software from Phenix[22], we improved the accuracy of the model fitting. We calculated the Q-score[23] from fitted models for density resolvability for protein and quantitative evaluation. At the 3.0 Å filtered map, the Q-score value for each candidate sequence was compared to the average Q-score value to determine the best candidate.

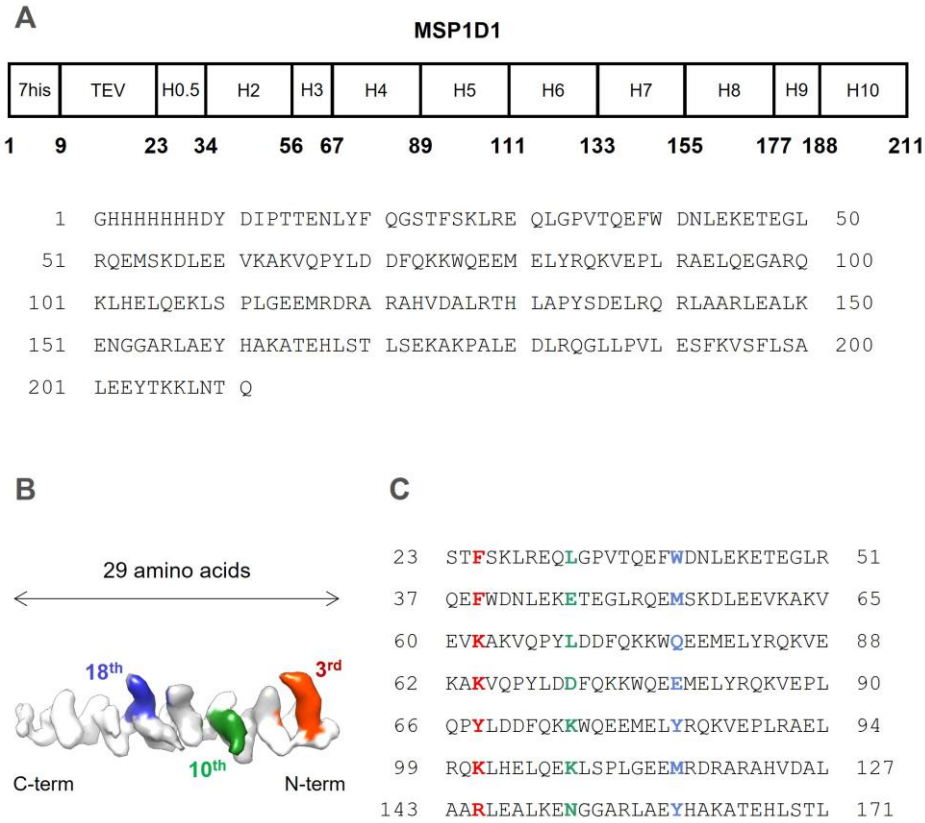

Figure 7. The amino acid sequence of MSP1D1 and candidates used for model fitting.

(A) MSP1D1 construct map and full amino acid sequences. (B) Partial high-resolution MSP map of cytochrome bd-I oxidase. MP-MSP contact side is shown, with the C-terminal end on the left and the N-terminal end on the right. Colored residues are bulky side chain density maps used as a reference for selecting candidate sequences for model fitting. (C) Seven candidate sequences were tried for the model fitting into the MSP high-resolution map.

2.6. Particle classification and 3D reconstruction by MSP resolution

This analysis was carried out with CryoSPARC, with the first 3D reconstruction of the V-ATPase V_0 complex done in RELION 3.0[22] with 2.81 Å resolution. The 3D classification includes 476k processed particles and the map from CryoSPARC, and the mask of the nanodisc region of the V_0 complex depicted using Chimera. The regularization parameter T of 4 was used with no image alignment. The resulting classes were categorized by whether the MSP strands were visible or not. The high-resolution MSP group had 203,419 particles (42.75% of total particles) while the low-resolution MSP group had 272,394 particles (57.25%). Using the NU-refinement program from CryoSPARC, three sets of 3D reconstruction were performed, with a total number of particles, the high-resolution MSP group, and the low-resolution MSP group. The input volume used was the same as the map used in RELION. The resulting output volume and the mask of only the MP region were used as input for the local refinement process in RELION to improve local resolution in the MP region. The total particles group had a final resolution of 2.86 Å, the high-resolution group had a final resolution of 2.92 Å, and the low-resolution group had a final resolution of 2.99 Å.

2.7. Local resolution analysis by MSP resolution

In CryoSPARC, we calculated the local resolution of the MSP using the output volume and mask derived from local refinement. In Chimera, MSP surface coloring was done from the output volume from the local refinement process. The local resolution output volume is entered as the input volume data value. The Color key was set in five intervals where the interval values were set to 2.5, 2.9, 3.3, 3.6, and 3.9 Å.

2.8. B-factor analysis by MSP resolution

In Phenix, we performed real-space refinement with default settings with V-ATPase V_0 complex map and model (6M0S) as the input. From this we obtained the atomic displacement parameter value (B-factor) for each residue in the protein.

2.9. Measuring the length of membrane protein hydrophobic region

We used PDBTM (http://pdbtm.enzim.hu/) to identify the transmembrane (TM) region of each MP. Using UCSF Chimera, we estimated the longest length of the TM region.

Chapter 3

Results

3.1. Asymmetric localization of membrane protein inside nanodisc

3.1.1. Analysis to identify the heterogeneous structure of protein-embedded nanodisc

To study the effect of the nanodisc on the membrane protein (MP) structural stabilization, we obtained datasets from EMPIAR of various MP structures purified in nanodisc to re-analyze each via focused refinement on the nanodisc itself (Table 1). For this, we first reprocessed all MP structures to published resolution and then performed 3D Variability Analysis (3DVA) with a tight mask applied around the nanodisc region (Fig. 8A).

Traditionally, MPs were thought to stabilize at the center of a relatively rigid nanodisc structure. In reality, however, MPs embedded within nanodisc are freely allowed to move within the phospholipid bilayer environment created by the nanodisc that is also constantly changing its shape as the MSP surrounding the lipids move as well. To analyze and study the structural behavior of proteins embedded in nanodisc, we need to classify various states that exist within a dataset. 3DVA allows us to classify the complex, heterogeneous collection of movements of MP and MSP into orthogonal sets of simpler movements that we can analyze individually. For instance, a “mode” created from 3DVA isolates a set of states where the MP moves linearly within a stable nanodisc. When analyzed separately but compiled together, these orthogonal modes can explain the entire complex movements that occur within

the nanodisc.

In all MPs that we studied, 3DVA revealed that protein can be distributed in various regions of the nanodisc, including at the edge where the protein makes direct contact with the MSP (Fig. 8C, 8D). Furthermore, we observed changes in the shape of the nanodisc, where the MSP adopts an elliptical shape with various degrees of ellipticity. The overall volume of the nanodisc is conserved during this process. We observed that for most proteins, the MP makes contact with MSP when the MSP adopts the lowest degree of ellipticity (Fig. 8E).

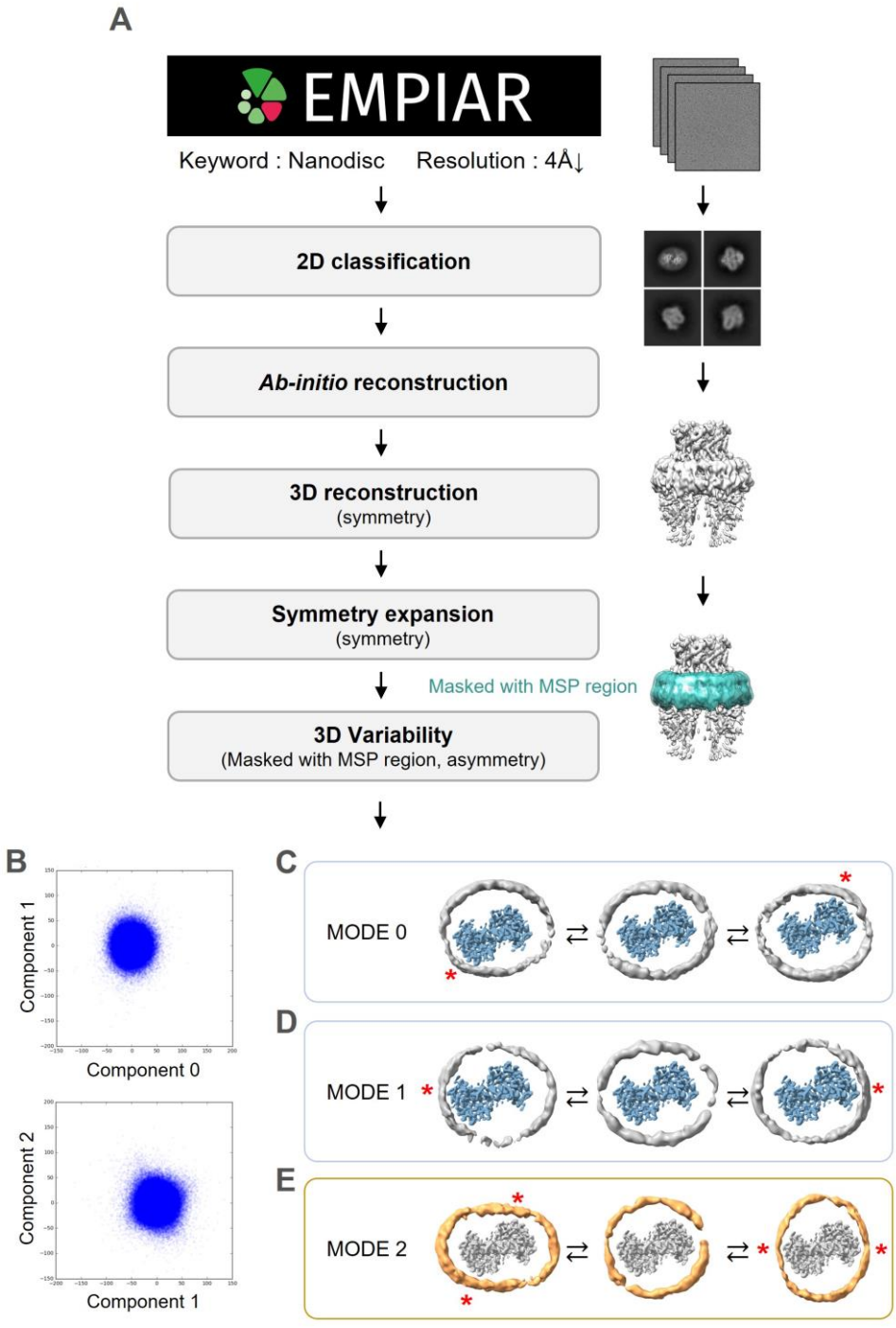

Figure 8. Analysis of heterogeneous structure of nanodisc

(A) Data processing workflow using CryoSPARC for 3DVA analysis. Among the MP used in the analysis, TMEM16A is shown as a representative protein. (B) 2D scatter plots of 3D latent coordinates of individual particles are solved by 3DVA. The scatter plots indicate the particles along each dimension. (C)(D)(E) Three representative modes of movement are identified through 3DVA. Asterisks refer to the contact point of MP–MSP. In modes 0 and 1, only the position of the MP is changed while maintaining the overall shape of the nanodisc. In mode 2, the entire shape of the nanodisc is deformed.

3.1.2. Quantitative analysis of protein embedded nanodisc and comparison of empirical vs homogeneous particle distribution

Assuming that the stability of a conformation is directly related to how populated that conformation is in the dataset, we devised a quantitative model to analyze this stability. Specifically, we compared the population of each conformation from the empirical dataset with a model in which each conformation is assumed to be equally populated (by random distribution of MPs within the nanodisc).

Three variables could be considered for a quantitative model of the MP movement within a nanodisc that deforms into an ellipse: R, C and Θ. R refers to the distance between the center of mass of the nanodisc and that of the MP (Fig. 6). Thus, as an example, if the protein is situated in the middle of the nanodisc, R = 0. The variable C refers to the focal value of the nanodisc. We assumed the shape of the nanodisc to be an ellipse with a specific value of foci that determines the degree of ellipticity of the nanodisc within a dataset. Θ refers to the angle between the center of mass of the nanodisc and that of the MP. While the variability in Θ is a realistic possibility, we did not observe this phenomenon during the 3DVA of our proteins. Therefore, this was not considered in our analysis. We either set R or C as the variable and normalized for either value. (nR, nC) Overall, for the case where the protein is moving around the nanodisc, we observed that the protein was more populated for $0 < nR < 2$ and $8 < nR < 10$ compared to the result if we assumed

that the distribution would be random (Fig. 9A). This indicates that the MP is most stabilized at the center and the edge of the nanodisc. As we will discuss in later sections, the stabilization at the edge is achieved through a direct interaction between the nanodisc and the MP.

In the other case, where the nanodisc deforms in an elliptical shape, we allowed the normalized value of C to vary. In our result, the nanodisc is stabilized when it makes direct contact between MP and MSP. This occurs not when the nanodisc adopts a traditional circular shape (C=0) but rather when the C value is maximized and the degree of ellipticity is the lowest (Fig. 9B).

In all cases of our analysis, data indicates that the MP is more populated and thus prefers when it makes direct contact with MSP. From this, we deduced that perhaps the contact between MSP and MP creates a stabilizing interaction. The nature of this interaction may not necessarily be specific, but it may be enough to disrupt the salt-bridge interaction between the MSP bilayer.

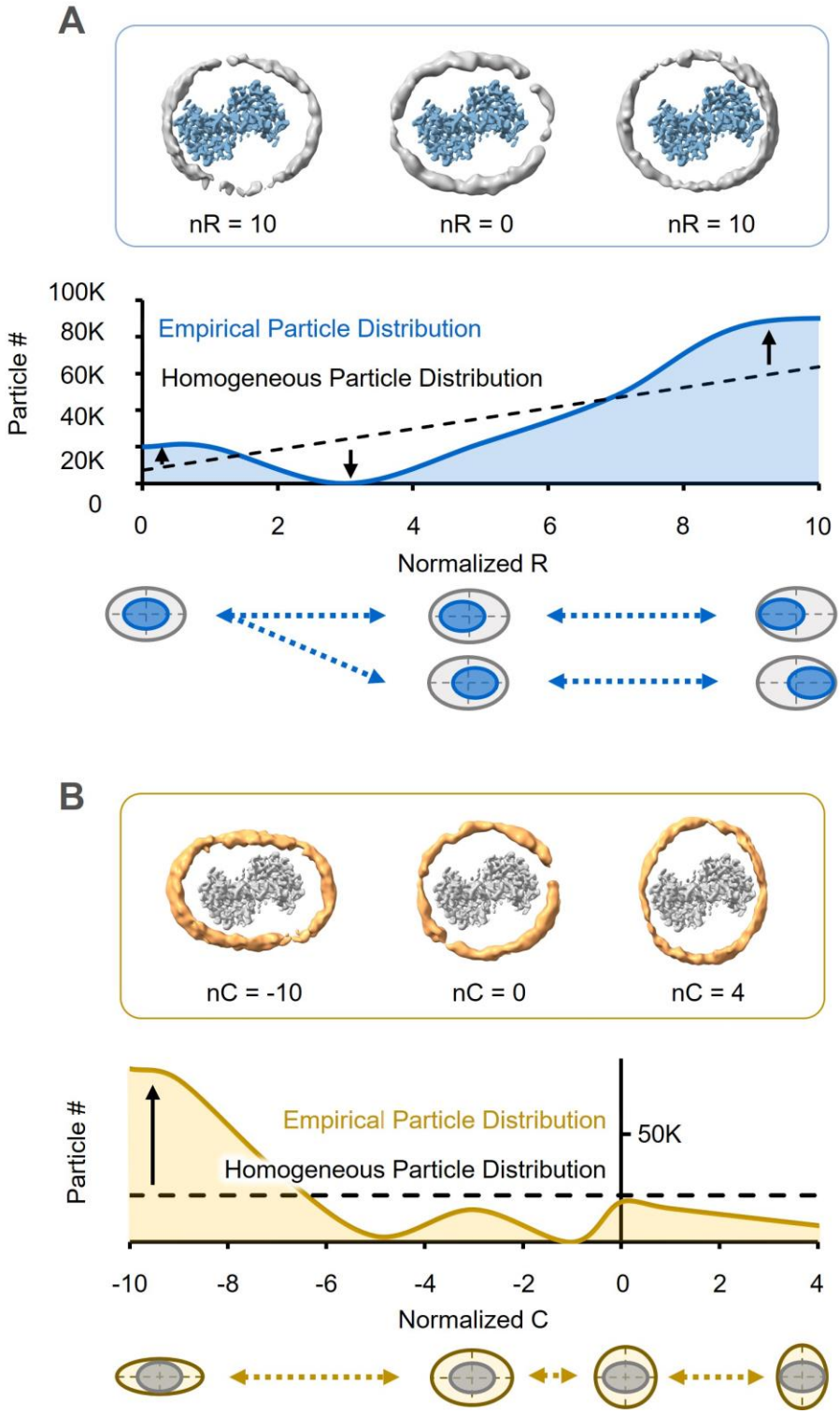
A
nR = 10
nR = 0
nR = 10
100K
80K
60K
40K
20K
0
Particle #
Empirical Particle Distribution
Homogeneous Particle Distribution
0
2
4
6
8
10
Normalized R
B
nC = -10
nC = 0
nC = 4
Particle #
Empirical Particle Distribution
50K
Homogeneous Particle Distribution
-10
-8
-6
-4
-2
0
2
4
Normalized C

Figure 9. Comparison of empirical vs homogeneous particle distribution

3DVA results of TMEM16A with two different variables. Both figures show the structure (top) and particle distribution graph (bottom) corresponding to each variable. A cartoon of the structure corresponding to the consideration of each variable is also shown. (A) For variable ‘nR’, MP is more localized on either the center or the edge of the nanodisc compared to the homogeneous distribution of particles. (B) For variable ‘nC’, MSP tends to deform horizontally more readily, following the shape of the MP.

3.2. Direct interaction observed between MSP and cytochrome bd-I oxidase

3.2.1. Surface charge on membrane protein and localization MSP

To identify the basis for the MP-MSP interaction, we overlapped the MSP on top of the surface charge map of the MPs that were solved using nanodisc. In all cases, the MSP strands were found in the hydrophobic edge region of the MP (Fig. 10). The initial MSP-MSP interaction in the nanodisc was altered to MSP-MP interactions. As a result, the MSP moved to the hydrophobic edge of the MP. With cytochrome bd-I oxidase as the MP, the large hydrophobic region of the MP widened the MSP double layer distance to the point where there is no longer interaction between the two MSP strands (Fig. 10). From this analysis, we observed that all protein embedded nanodisc showed that the interactions between the MSP strands can be converted into an MP-MSP interaction. The fact that MSP is moved specifically to the hydrophobic edge of the MP suggests that there are specific residue-to-residue interactions that form in the process.

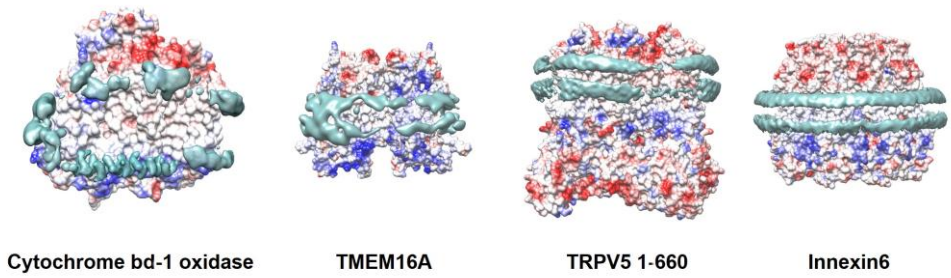

Figure 10. MSP mapping on the Surface charge of MP

Four representative proteins were used for analysis. MP surface charge and location of MSP (sky blue) are shown. In all four cases, MSP moves towards the hydrophobic edge of the MP.

3.2.2. Partial high-resolution MSP model fitting and MP-MSP interaction analysis

The cytochrome bd-I oxidase map with a 3 Å low-pass filter exhibited a partially high-resolution MSP map (Fig. 11A, B). From this, we sought the specific interactions between MP-MSP. For model fitting, we isolated a partial high-resolution MSP map. For the site of specific interactions, candidate sequences were chosen from MSP1D1 that may fit into the high-resolution map. Considering that the high-resolution map exhibited eight α-helical turns, we designated the candidate sequences to be of length 29 amino acids (3.6 amino acids per turn x 8 turns). In the MSP map, residues 3, 10, and 18 had large bulky side chain densities (Fig. 7B). Therefore, any sequences that had small residues such as alanine, valine, glycine, or proline were immediately discounted. Through this process of elimination, seven candidate sequences were created, and all seven were tried for model fitting (Fig. 7C) (Fig. 11D, F). Using the Q-score, which is a quantitative parameter for the quality of model fitting, we compared the fit on each of the other seven candidate sequences. Sequence 37-65 (QEFWDNLEKETEG LRQEMSKDLEEVKAKV) showed the highest residue Q-score, which shows the overall resolvability score for each atom and backbone. At the 3 Å filtered map, this sequence also was the closest to the expected Q-score of 0.5 (Fig. 11E).

Once the sequence corresponding to the high-resolution map of the MSP interacting with MP was identified and fitted, we

sought to characterize the specific interactions with the MP itself. MP-MSP hydrophobic interactions included L42-L43, W360-V61 while the hydrophilic interactions included Q125-D57 and K361-D57 respectively (Fig. 11C). As a result, amphipathic interactions stabilize the MP-MSP contact.

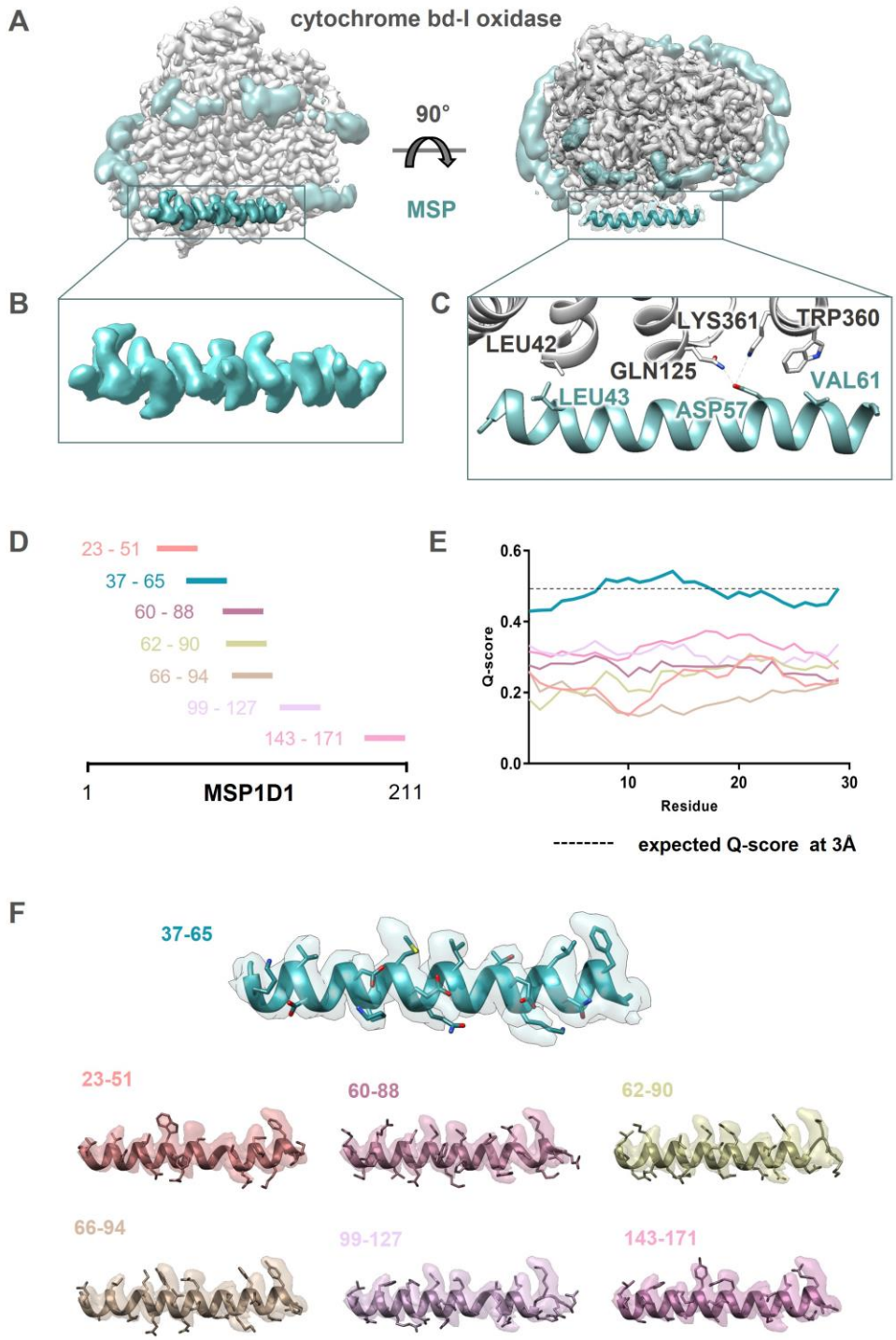

Figure 11. Partial high-resolution MSP and model fitting

(A) Side and top view of cytochrome bd-I oxidase. (B) A close-up of the partial high-resolution MSP map (C) MSP sequence 37-65 with the highest Q-score and MP interaction site. Hydrophobic interaction and charge-charge interaction can both be observed. (D) Schematic diagram of seven candidate sequences used for analysis. (E) Average Q-score graph for each candidate. The dotted line indicates the expected Q-score at a 3 Å low-pass filter. Only the candidate sequence 37-65 has a score close to the expected Q-score. (F) Docking of all candidate sequences into the partial high-resolution MSP map.

3.3. Stabilization of membrane protein induced by direct interaction with MSP

3.3.1. Classification according to MP-MSP direct interaction

To study the impact of the MP-MSP interaction on the MP itself, we looked at the nanodisc-reconstituted structure of the V-ATPase V_0 complex as a model. Unlike many other MPs we studied, the V_0 complex showed a clear separation between a class where individual MSP strands are distinguished and a class where they are not upon masking with MSP and undergoing focused classification (Fig. 12A). The class with clearly visible MSP strand had MP-MSP interaction while the one without a clear distinction of the strands had no interactions. Thus, analysis of each class of V-ATPase V_0 complex would reveal the nature of the MP-MSP interaction. 3D reconstruction of the V-ATPase V_0 complex with the nanodisc region yielded a 2.82 Å map from 475,813 particles. Then we performed a focused classification using a mask derived from the nanodisc region to classify the MSP densities as described above. Among the eight classes, three classes comprising 203,419 particles (42.75% of the total number of particles) exhibited clear MSP strands in their maps (i.e. high-resolution MSP classes) while five classes comprising 272,394 (57.25% of the total number of particles) exhibited blurry or obscure MSP strand densities in their maps (i.e. low-resolution MSP classes). Thus, the high-resolution MSP classes had ~14.5% fewer particles in number compared to the low-resolution MSP classes. For our analysis, we considered

three groups: MP-MSP interacting particles group (group I), MP-MSP not interacting particles group (group N), and the total particles group (group T) (Fig. 12A).

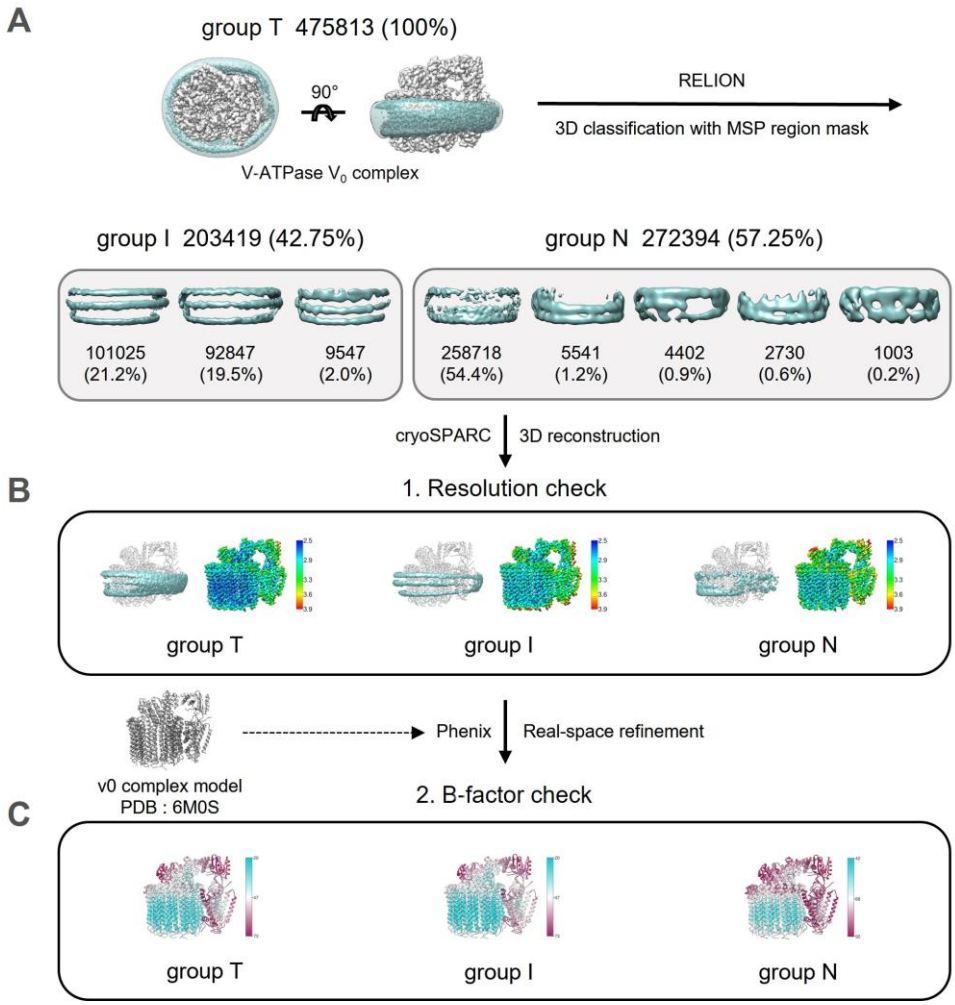

Figure 12. The overall workflow of membrane protein stabilization analysis induced by direct interaction with MSP

(A) 3D-focused classification yields high (group I) and low-resolution (group N) MSP classes that reveal both classes with and without MP-MSP interaction. Classification with the entire dataset is designated as group T (B) Resolution comparison of MP from each group. 3D reconstruction map for each (left) and local resolution colored map (right) are shown. MP is shown as gray, while MSP is shown as light blue. (C) B-factor coloring for each class of V-ATPase V_0 complex.

3.3.2. Analysis of the effect of MP-MSP direct interaction on the resolution

We studied the effect of the MP-MSP interaction on the resolution of the MP by focusing our groups T, I and N on the MP region. 3D reconstruction of groups T, I and N using a mask of the MP region resulted in an average resolution of 2.86 Å, 2.92 Å and 2.99 Å, respectively (Fig. 13). The fact that the average resolution of all three groups was similar indicates that the group N is not composed of junk particles with low-resolution MP but rather composed of only particles with low MSP resolutions. For a comparison of the MP-MSP direct interaction between each group, we looked at the local resolution for each group.

The TM region of the MP showed similar local resolutions between group I and N at 2.8 Å resolution while the group T with twice as many particles showed a slightly higher resolution at 2.5 Å. Since the TM region is embedded in phospholipids and is less affected by the MSP itself, the effect of the number of particles in the processing may be more significant than the effect of the MSP resolution on the overall local resolution (Fig. 13).

All three groups exhibit similarly high MP local resolution on the luminal side of the TM edge. This may also be because this region of the MP also doesn't become stabilized from the interaction with MSP itself. In contrast, the cytosolic side of the TM edge MP local resolution shows a distinct difference in resolution. Group I with the highest MSP resolution and group T with the most particle

number have local resolution in the cytosolic region of 3.0 Å, while group N shows a local resolution of 3.5 Å in this region (Fig. 13). With this, we can deduce that the MP–MSP direct interaction improves the local resolution of MP.

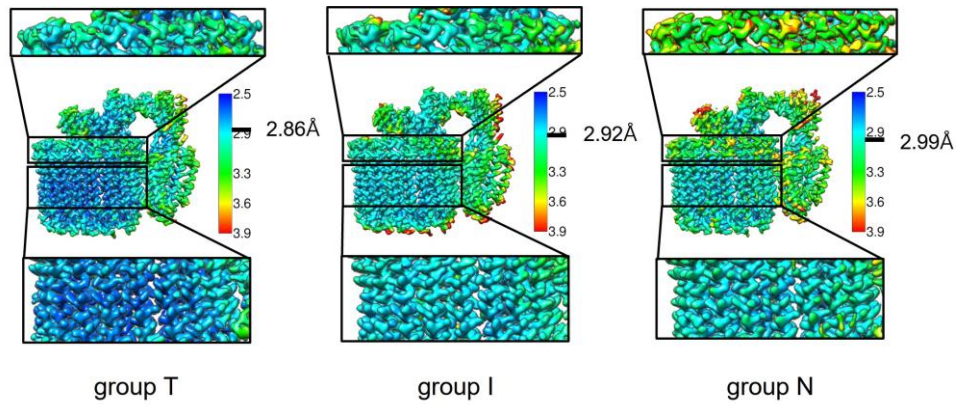

Figure 13. Local resolution of membrane protein from each group

Final V-ATPase V_0 complex 3D density map for each group colored by their local resolution. Zoomed-in view of the MP local resolution near the MSP (top) and PL (bottom). Average resolution is indicated on the scale bar.

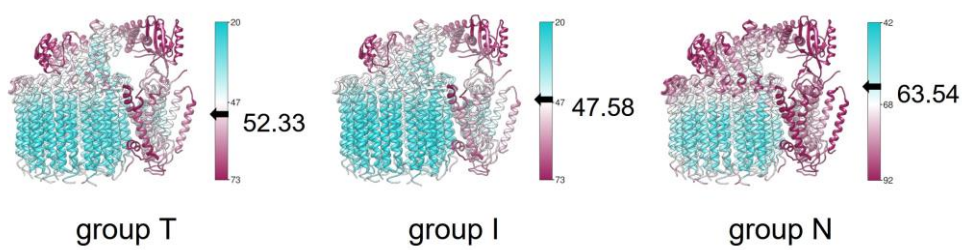

Figure 14. B-factor of membrane protein from each group

Post-refinement model of the V-ATPase V_0 complex categorized by each group (T, I, and N). Models are colored according to residue-by-residue B-factor values. Average B-factor value is indicated on the scale bar.

3.3.3. Analysis the effect of MP-MSP direct interaction on B-factor

The impact of the MP-MSP interaction on the MP B-factor was further studied using the V-ATPase V_0 complex model. Maps from groups T, I, N were used for model fitting and further refinement. The average B-factor for the three groups T, I, N were 52.33, 47.58, and 63.94, respectively (Fig. 14). The fact that the average B-factor for group I was the lowest even compared to group T, which has twice as many particles, indicates that MP-MSP interaction is involved in the lowering of the B-factor and thus stabilization of MP structure.

From our earlier analysis of local resolution, we saw that MP-MSP interaction affects the resolution of the local region of direct interaction more than overall MP resolution. Thus, we sought to look at the effect of the direct interaction on the B-factor as well. In order to limit the variance arising from differences in residues in the MSP interaction, we compared the B-factor of chains E, F, G, H, I, J, K and L which have identical sequences but only differ in how and if they interact with the nanodisc and MSP (Fig. 15A, B). For instance, chains E, F, G, H, I, and J make direct interactions with MSP, chain K interacts directly with the phospholipid, and chain L interacts directly with another subunit of V-ATPase V_0 complex. To evaluate the degree of stabilization arising from MSP interaction, we compared the difference in B-factor between groups I and N (ΔB-factor). The larger the amplitude of ΔB-factor for a

particular residue, the more stabilizing the MSP interaction is on the MP. For each residue within each chain, ΔB-factor resulted in a positive value, indicating that the MSP interaction also stabilizes the overall B-factor of the MP.

In chain K and L where MP does not interact directly with MSP, ΔB-factor values for each residue were quite similar (Fig. 16B). Even among chains that interact with MP, chains H, I, and J display little deviations from their average ΔB-factor values. Only chains E, F, and G, located near the top and middle strands of the MSP, displayed significant deviations in ΔB-factor values from their average. We highlight these differences in Figure 16B, C. This indicates that even among MP residues interacting with MSP there are specific regions that seem to stabilize even further. To tease out this feature using further analysis, we evaluated the average ΔB-factor for all residues for each chain and searched for residues where the ΔB-factor was above the average value. In the luminal side of the TM, the value was below average for each residue. This may be because this is the region where the difference in MSP direct interaction is not significant. In the cytosolic region where there is a significant difference in MSP direct interaction, ΔB-factor for these residues were above the average value. (Fig. 16C) Thus, MSP direct interaction stabilizes the B-factor on a residue-by-residue basis.

To summarize, MP-MSP interaction stabilizes the overall structure of MP but specifically the directly interacting residues

seem to exhibit especially further stabilization indicated by lower B-factor and higher resolution.

A

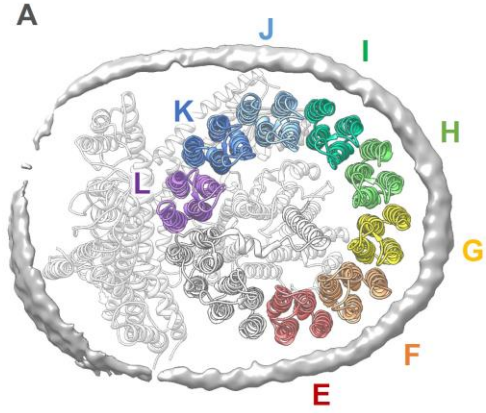

B

```
chain E    1 MTELCPVYAPFFGAIGCASAIIFTSLGAAYGTAKSGVGICATCVLRPDLLFKNIVPVIMA 60
chain F    1 MTELCPVYAPFFGAIGCASAIIFTSLGAAYGTAKSGVGICATCVLRPDLLFKNIVPVIMA 60
chain G    1 MTELCPVYAPFFGAIGCASAIIFTSLGAAYGTAKSGVGICATCVLRPDLLFKNIVPVIMA 60
chain H    1 MTELCPVYAPFFGAIGCASAIIFTSLGAAYGTAKSGVGICATCVLRPDLLFKNIVPVIMA 60
chain I    1 MTELCPVYAPFFGAIGCASAIIFTSLGAAYGTAKSGVGICATCVLRPDLLFKNIVPVIMA 60
chain J    1 MTELCPVYAPFFGAIGCASAIIFTSLGAAYGTAKSGVGICATCVLRPDLLFKNIVPVIMA 60
chain K    1 MTELCPVYAPFFGAIGCASAIIFTSLGAAYGTAKSGVGICATCVLRPDLLFKNIVPVIMA 60
chain L    1 MTELCPVYAPFFGAIGCASAIIFTSLGAAYGTAKSGVGICATCVLRPDLLFKNIVPVIMA 60

chain E   61 GIIAIYGLVVSVLVCYSLGQKQALYTGFIQLGAGLSVGLSGLAAGFAIGIVGDAGVRGSS 120
chain F   61 GIIAIYGLVVSVLVCYSLGQKQALYTGFIQLGAGLSVGLSGLAAGFAIGIVGDAGVRGSS 120
chain G   61 GIIAIYGLVVSVLVCYSLGQKQALYTGFIQLGAGLSVGLSGLAAGFAIGIVGDAGVRGSS 120
chain H   61 GIIAIYGLVVSVLVCYSLGQKQALYTGFIQLGAGLSVGLSGLAAGFAIGIVGDAGVRGSS 120
chain I   61 GIIAIYGLVVSVLVCYSLGQKQALYTGFIQLGAGLSVGLSGLAAGFAIGIVGDAGVRGSS 120
chain J   61 GIIAIYGLVVSVLVCYSLGQKQALYTGFIQLGAGLSVGLSGLAAGFAIGIVGDAGVRGSS 120
chain K   61 GIIAIYGLVVSVLVCYSLGQKQALYTGFIQLGAGLSVGLSGLAAGFAIGIVGDAGVRGSS 120
chain L   61 GIIAIYGLVVSVLVCYSLGQKQALYTGFIQLGAGLSVGLSGLAAGFAIGIVGDAGVRGSS 120

chain E  121 QQPRLFVGMILILIFAEVLGLYGLIVALLLNSRATQDVV 159
chain F  121 QQPRLFVGMILILIFAEVLGLYGLIVALLLNSRATQDVV 159
chain G  121 QQPRLFVGMILILIFAEVLGLYGLIVALLLNSRATQDVV 159
chain H  121 QQPRLFVGMILILIFAEVLGLYGLIVALLLNSRATQDVV 159
chain I  121 QQPRLFVGMILILIFAEVLGLYGLIVALLLNSRATQDVV 159
chain J  121 QQPRLFVGMILILIFAEVLGLYGLIVALLLNSRATQDVV 159
chain K  121 QQPRLFVGMILILIFAEVLGLYGLIVALLLNSRATQDVV 159
chain L  121 QQPRLFVGMILILIFAEVLGLYGLIVALLLNSRATQDVV 159
```

Figure 15. Chains of V−ATPase V_0 complex used for analysis

(A) Bottom view of V−ATPase V_0 complex and MSP. Chain E~J are in contact with MSP, chain K is in contact with PL, and chain L is in contact with another subunit of MP. (B) Sequence alignment of chains E~L. All sequences are identical.

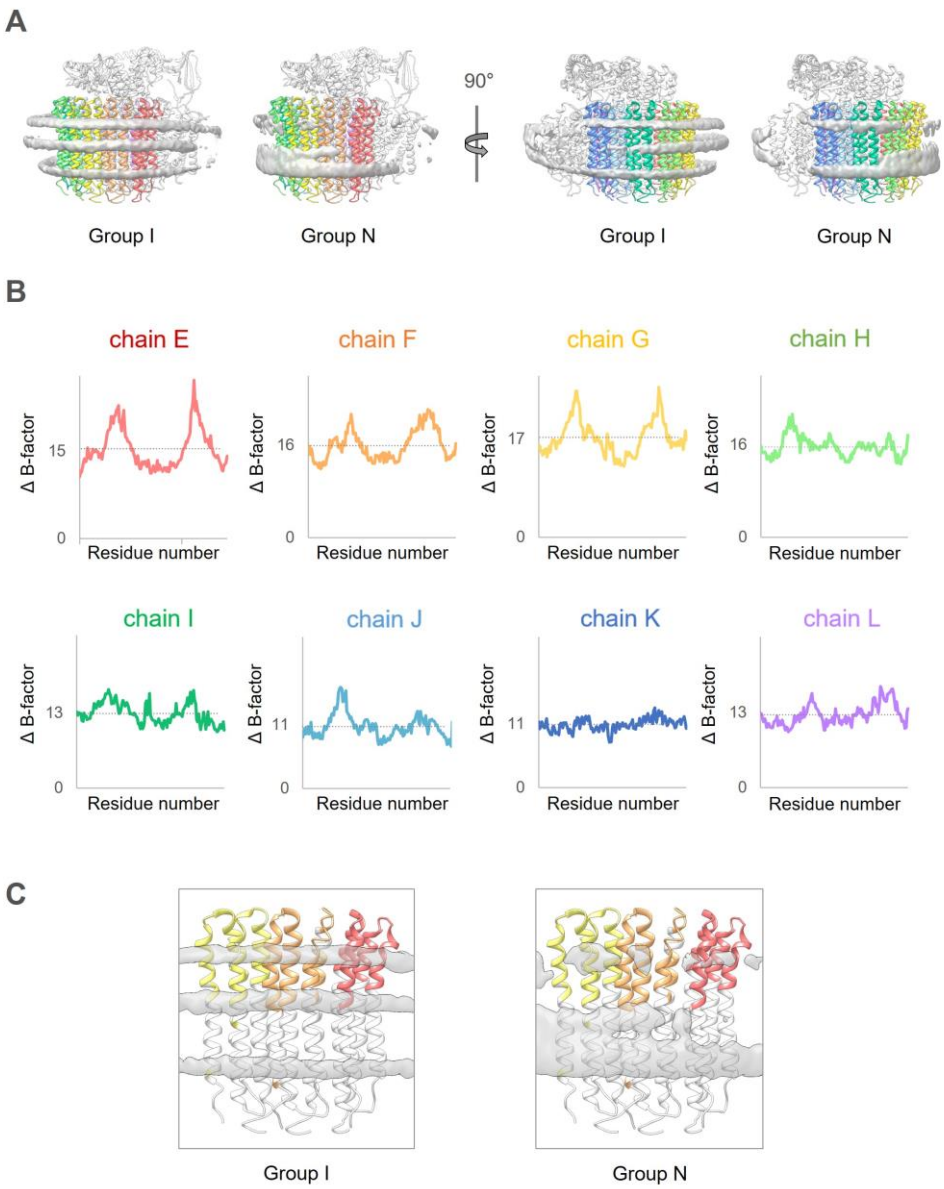

Figure 16. ΔB-factor analysis of each chain of V-ATPase V_0 complex

(A) Right and left side views of group I and N. Chains on the left side show significant difference in resolution of MSP between group I and N. Chains on the right-side show less difference in MSP resolution between the two groups. Right side shows similar resolution between top and bottom MSP

strands. (B) ΔB-factor values by chain. The dotted gray line indicates the average ΔB-factor for each chain and the colored line shows the ΔB-factor values by residue. (C) Zoomed-in view of chain E, F, and G from group I (left) and N (right). Light gray density map indicates the MSP density. Colored region indicates the residues exceeding the average ΔB-factor values for each chain. Areas with the largest differences in MSP resolution also showed above-average ΔB-factor values.

3.4. MSP can form a three-stranded structure around the membrane protein hydrophobic region for further stabilization

3.4.1. Correlation analysis between the hydrophobic region width of membrane protein and the number of MSP strands

Unlike most proteins in our study, the V-ATPase V_0 complex exhibited three rather than two strands of MSP surrounding the nanodisc. We also identified two other MP glucosyltransferase Alg6 (PDB 6SNI, EMD-10258), Arabinofuranosyltransferase Aft (PDB 6W98, EMD-21580) that show three strands of MSP in the nanodisc. To see if this behavior is dependent on the MP itself, we estimated the length of the TM region of each protein we studied as that could give us information about how far and how many MSP strands can envelope the MP (Fig. 17). The TM length of the V-ATPase V_0 complex is 45.76 Å, of Alg6 is 43.21 Å, and of AftD is 48.24 Å. The TM lengths of other MPs with two strands of MSP when reconstituted in nanodisc are as follows: TRPM4 (PDB 6BQV) 31.686 Å, TRPV1 (PDB 5IRX) 32.58 Å, TMEM16F (PDB 6P48) 33.89 Å, Innexin6 (PDB 6KFH) 34.484 Å, TRPV5 W583A (PDB 6O1U) 35.45 Å, TRPV5 1-660 (PDB 6O1N) 35.567 Å, TMEM16A (PDB 6BGI) 37.525 Å, LRRC8A (PDB 6NZW) 38.126 Å, and afTMEM16 (PDB 6E1O) 40.264 Å. The range of TM lengths for the MPs exhibiting three MSP strands in nanodisc is 43-48 Å, while that for the MPs exhibiting two MSP strands is 31-40 Å. Considering that the diameter of an α-helix is ~5 Å and that MSP

requires minimal distance between each helix, we propose that the additional layer of MSP is introduced when a certain threshold of TM length is reached to allow the third strand to be added for further overall stabilization.

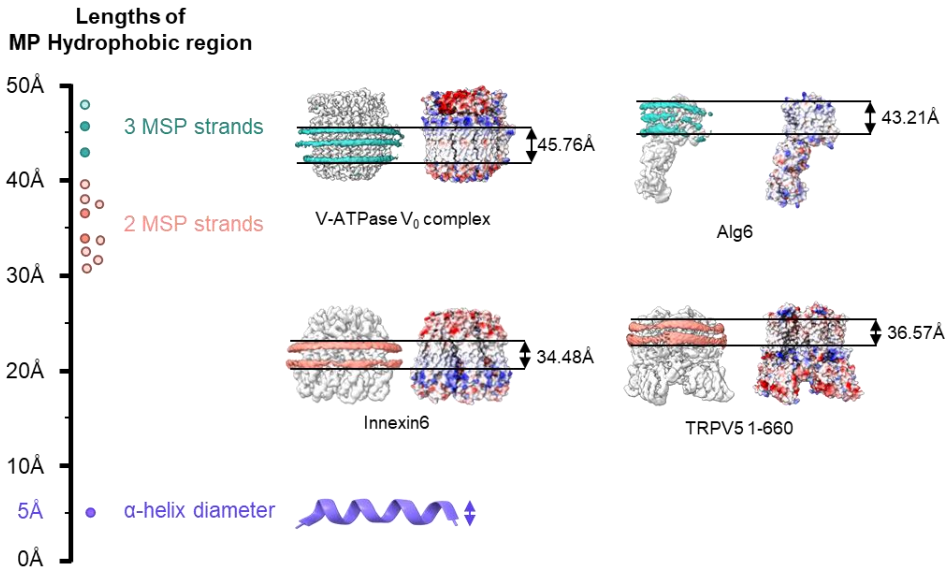

Figure 17. Measurement of membrane protein hydrophobic region length

Measurement of the MP length of proteins from Table 1. Each dot in the graph indicates each protein in our analysis pipeline. Mint-colored dot indicates proteins with three strands of MSP, while the orange-colored dot indicates proteins with two strands of MSP. The purple dot indicates the diameter of the alpha-helix, corresponding to the length of one strand of MSP as a reference. The filled-in dots correspond to the corresponding proteins shown on the right. V-ATPase V_0 complex and Alg6 proteins exhibit three strands of MSP in their structures, while Innexin6 and TRPV5 exhibit two strands. For each protein, the left figure shows the 3D reconstructed map while the right shows the map colored by surface charges. The distance between the top and bottom strands of the MSP matches with the TM length of the MP. As a result, MPs with three strands of MSP have longer TM length compared to those with only two strands.

Chapter 4

Discussion

This thesis sought to explore the stabilizing effect of the nanodisc structure on the membrane protein (MP). Firstly, we observed the heterogeneous nature of the nanodisc through 3D Variability Analysis (3DVA), and using a quantitative model, we analyzed the particle distribution in individual datasets to assess what state stabilizes the MP. We observed that there was a significantly higher number of distributions of states where the MP is in contact with the MSP. Secondly, we identified the surface charge of the MP and looked at the relative location of the MSP to characterize these contacts more in detail. We observed that for all cases we studied, the MSP moved to the hydrophobic edge of the MP. This movement destabilized the salt bridge interaction between the MSP strands as the distance between the two strands increased. As observed in high-resolution parts of the site of MP-MSP interaction, each strand of MSP instead formed hydrophobic and charge-charge interactions with the MP. Lastly, we looked at the effect of these MP-MSP interactions on the overall stability of the MP by looking at the local resolution and B-factor where the interactions occurred. We observed that the MP-MSP direct interaction improves the local resolution of the MP and stabilizes the B-factor on a residue level.

From our findings, we propose a mechanism of MP stabilization from nanodisc in the following way (Fig. 18). During the initial formation of the nanodisc, the hydrophobic region of the MP is surrounded by the phospholipid bilayer, which is stabilized by the surrounding MSP proteins. MSP strands are initially stabilized

by the salt bridges, but continuous exchange of interactions lead to a horizontal movement. Meanwhile, the MP is allowed to freely diffuse within the nanodisc enveloped by the phospholipid. When the MP moves the edge of the nanodisc and comes in contact with the surrounding MSP, the MSP–MSP strand interaction is altered into an MP–MSP interaction. In this process, the two strands of MSP move vertically to the TM edge of the MP. Due to the amphipathic nature of MSP, both hydrophobic and charge–charge interactions form between MP and MSP, forming the stabilized MP embedded nanodisc.

As the two strands of MSP move to the hydrophobic edge of the MP, the hydrophobic TM region of the MP can be exposed to aqueous solution, which may destabilize the protein. To accommodate for this, a third MSP strand may form to surround this exposed hydrophobic region for stabilization. Thus, depending on the TM length of the MP, the MSP may adopt three strands rather than two for stabilization.

The main limitation of our study is that we used different proteins for each stage of our analysis. For instance, we used an extensive number of various nanodisc–embedded MPs to study the heterogeneous nature of the nanodisc. However, these proteins were not used to study the MP–MSP interaction or the impact of these interactions on the B–factor and the resolution of the MPs. The reasoning for this is that we required datasets of MPs that met the specific needs for each analysis. For example, for our analysis

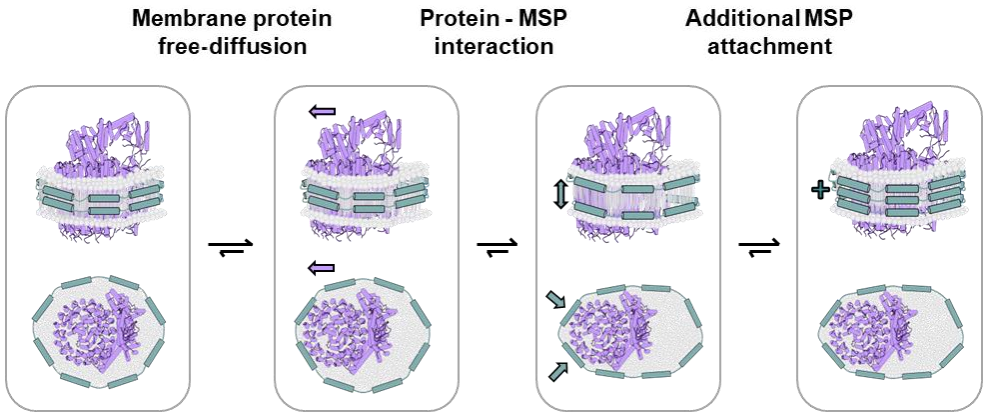

Figure 18. Schematic illustration of membrane protein stabilization by MSP

Schematic illustration depicting the nanodisc stabilization process after initial assembly. MSP bilayer (green) envelops MP (purple) and PL (gray), supported by salt-bridge interactions between the MSP strands. MP undergoes diffusive movement within the nanodisc and MP and MSP are allowed to make contact. Here, MSP-MSP salt-bridge interaction is converted to MP-MSP interactions. The overall nanodisc adopts an elliptical shape during this process. If the MP has a TM length above a certain threshold, two strands of MSP come far enough apart to allow for the presence of a third strand of MSP, which allows for further stabilization of the MP through MP-MSP contacts.

of particle distribution to study the localization of MPs within the nanodisc and the changes in the shape of the nanodisc, we only required datasets of MPs reconstituted in nanodisc. For the analysis of the MP–MSP interaction, we needed datasets that displayed MP–MSP direct interactions at a high–resolution (i.e. high resolution contact map of MSP). To study the effect of the MSP interaction on the MP, the dataset needed to have solely MP–MSP interactions without other extraneous interactions. Lastly, the analysis of the correlation between the number of MSP strands surrounding the nanodisc and the TM length of the MP required nanodisc datasets with three strands of MSP. For these reasons we used different samples for each area of our analysis, but this does not mean that our results are only limited to the proteins we studied. In fact, we propose that the phenomena we observed could be applied more generally to MPs reconstituted in nanodiscs.

In all of the samples we studied, the MSP moved to the hydrophobic edge of the MP once the MP came in contact with the MSP. This indicates that there are interactions that form between MP and MSP. However, most datasets did not exhibit a high–resolution MP–MSP interaction map due to the flexible structural characteristics of MSP. Furthermore, most MPs did not have sufficient TM length to clearly weaken the MSP–MSP interaction to form only MP–MSP interactions. Cytochrome bd–I oxidase dataset was an example that fulfilled all of these requirements. The TM length is sufficiently that MSP–MSP interaction is properly broken

to form MP-MSP interactions in the high-resolution map of the MSP. The MSP binding region is also quite flat without much curvature, which could prevent phospholipid from interfering with the proper MP-MSP interactions. Nonetheless, we observed that in all of the datasets of various MPs in nanodiscs, MP-MSP amphipathic contact is preferred where the MSP moves to the hydrophobic edge of the MP. This indicates that these proteins also exhibit hydrophobic and electrostatic interactions with the MSP, with different strengths of interactions.

For our analysis of local resolution and B-factor, we required a MP with properties that exhibit both MP-MSP interaction and no interaction from the same sequence. This was needed to isolate the effect of the MSP interaction on the MP by comparing the two cases. We assumed that the strength of MP-MSP interaction is directly correlated to the resolution of the MSP strand map as MSP would be more stabilized by the MP interaction. Most MPs showed low MSP resolution. In the V-ATPase V_0 complex, however, we were able to classify and identify both high- and low-resolution MSP strand maps. This may partially be due to the fact that the V-ATPase V_0 complex exhibits three strands of MSP rather than the usual two strands. With only two strands of MSP, the TM length of MP is short enough that the distance between the two MSP strands is also close. In this case, there is a constant exchange between MP-MSP and MSP-MSP interactions, making the densities of the individual strand map difficult to resolve.

With three strands, however, the TM length is long enough that MSP moves vertically more freely if it is not interacting with the MP. Furthermore, there are more possibilities of MP–MSP interactions with three strands of MSP. For these reasons, the V–ATPase V_0 complex in nanodisc with three strands of MSP was used to isolate the effect of the MSP–MP interaction. Intermolecular and intramolecular forces were observed to conclude that the direct interaction with the MSP stabilizes the MP. This result validated previous studies that indicated that the stabilization of MP via nanodisc allows for a high–resolution structure of the protein.

In summary, our study evaluated the MSP's stabilizing effect on the MP in nanodisc through the analysis of heterogeneous structure of the nanodisc and MP–MSP direct interactions. In truth, there are other methods to stabilize the MPs outside of their natural bilayer environment, such as reconstituting in detergent, amphipol and SMA lipid particles. We did not undergo extensive comparison with all of these various methods in this study, but it would be a useful analysis to highlight the stabilizing effect that nanodisc may have over other reconstitution methods. Furthermore, an extensive understanding of the microenvironment of the MP reconstituted in nanodisc would allow for the possibility for MSP engineering to accommodate for each MP. This could aid in the stabilization of even highly unstable MPs and thus allow for structural studies of such proteins.

References

1. Sanders, C.R., and Nagy, J.K. (2000). Misfolding of membrane proteins in health and disease: the lady or the tiger? Curr Opin Struct Biol *10*, 438–442. 10.1016/s0959-440x(00)00112-3.
2. Zampieri, V., Gobet, A., Robert, X., Falson, P., and Chaptal, V. (2021). CryoEM reconstructions of membrane proteins solved in several amphipathic solvents, nanodisc, amphipol and detergents, yield amphipathic belts of similar sizes corresponding to a common ordered solvent layer. Biochim Biophys Acta Biomembr *1863*, 183693. 10.1016/j.bbamem.2021.183693.
3. Sligar, S.G., and Denisov, I.G. (2021). Nanodiscs: A toolkit for membrane protein science. Protein Sci *30*, 297–315. 10.1002/pro.3994.
4. Gao, Y., Cao, E., Julius, D., and Cheng, Y. (2016). TRPV1 structures in nanodiscs reveal mechanisms of ligand and lipid action. Nature *534*, 347–351. 10.1038/nature17964.
5. Autzen, H.E., Julius, D., and Cheng, Y. (2019). Membrane mimetic systems in CryoEM: keeping membrane proteins in their native environment. Curr Opin Struct Biol *58*, 259–268. 10.1016/j.sbi.2019.05.022.
6. Reis, R.I., and Moraes, I. (2020). Probing Membrane Protein Assembly into Nanodiscs by In Situ Dynamic Light Scattering: A(2A) Receptor as a Case Study. Biology (Basel) *9*. 10.3390/biology9110400.
7. Denisov, I.G., and Sligar, S.G. (2017). Nanodiscs in

Membrane Biochemistry and Biophysics. Chem Rev *117*, 4669-4713. 10.1021/acs.chemrev.6b00690.

8. Klon, A.E., Segrest, J.P., and Harvey, S.C. (2002). Molecular dynamics simulations on discoidal HDL particles suggest a mechanism for rotation in the apo A-I belt model. J Mol Biol *324*, 703-721. 10.1016/s0022-2836(02)01143-9.

9. Pourmousa, M., and Pastor, R.W. (2018). Molecular dynamics simulations of lipid nanodiscs. Biochim Biophys Acta Biomembr *1860*, 2094-2107. 10.1016/j.bbamem.2018.04.015.

10. Lopez, C.A., Swift, M.F., Xu, X.P., Hanein, D., Volkmann, N., and Gnanakaran, S. (2019). Biophysical Characterization of a Nanodisc with and without BAX: An Integrative Study Using Molecular Dynamics Simulations and Cryo-EM. Structure *27*, 988-999 e984. 10.1016/j.str.2019.03.013.

11. Kratzer, A., Giral, H., and Landmesser, U. (2014). High-density lipoproteins as modulators of endothelial cell functions: alterations in patients with coronary artery disease. Cardiovasc Res *103*, 350-361. 10.1093/cvr/cvu139.

12. Yeh, V., Lee, T.Y., Chen, C.W., Kuo, P.C., Shiue, J., Chu, L.K., and Yu, T.Y. (2018). Highly Efficient Transfer of 7TM Membrane Protein from Native Membrane to Covalently Circularized Nanodisc. Sci Rep *8*, 13501. 10.1038/s41598-018-31925-1.

13. Hagn, F., Nasr, M.L., and Wagner, G. (2018). Assembly of phospholipid nanodiscs of controlled size for structural studies of membrane proteins by NMR. Nat Protoc *13*, 79-98. 10.1038/nprot.2017.094.

14. Puthenveetil, R., Nguyen, K., and Vinogradova, O. (2017).

Nanodiscs and Solution NMR: preparation, application and challenges. Nanotechnol Rev *6*, 111–126. 10.1515/ntrev-2016-0076.

15. Segrest, J.P., Jones, M.K., Klon, A.E., Sheldahl, C.J., Hellinger, M., De Loof, H., and Harvey, S.C. (1999). A detailed molecular belt model for apolipoprotein A-I in discoidal high density lipoprotein. J Biol Chem *274*, 31755-31758. 10.1074/jbc.274.45.31755.

16. Punjani, A., Rubinstein, J.L., Fleet, D.J., and Brubaker, M.A. (2017). cryoSPARC: algorithms for rapid unsupervised cryo-EM structure determination. Nat Methods *14*, 290-296. 10.1038/nmeth.4169.

17. Zheng, S.Q., Palovcak, E., Armache, J.P., Verba, K.A., Cheng, Y., and Agard, D.A. (2017). MotionCor2: anisotropic correction of beam-induced motion for improved cryo-electron microscopy. Nat Methods *14*, 331-332. 10.1038/nmeth.4193.

18. Rohou, A., and Grigorieff, N. (2015). CTFFIND4: Fast and accurate defocus estimation from electron micrographs. J Struct Biol *192*, 216-221. 10.1016/j.jsb.2015.08.008.

19. Pettersen, E.F., Goddard, T.D., Huang, C.C., Couch, G.S., Greenblatt, D.M., Meng, E.C., and Ferrin, T.E. (2004). UCSF Chimera--a visualization system for exploratory research and analysis. J Comput Chem *25*, 1605-1612. 10.1002/jcc.20084.

20. Punjani, A., and Fleet, D.J. (2021). 3D variability analysis: Resolving continuous flexibility and discrete heterogeneity from single particle cryo-EM. J Struct Biol *213*, 107702. 10.1016/j.jsb.2021.107702.

21. Croll, T.I. (2018). ISOLDE: a physically realistic environment for model building into low-resolution electron-density maps. Acta Crystallogr D Struct Biol *74*, 519-530. 10.1107/S2059798318002425.

22. Afonine, P.V., Klaholz, B.P., Moriarty, N.W., Poon, B.K., Sobolev, O.V., Terwilliger, T.C., Adams, P.D., and Urzhumtsev, A. (2018). New tools for the analysis and validation of cryo-EM maps and atomic models. Acta Crystallogr D Struct Biol *74*, 814-840. 10.1107/S2059798318009324.

23. Pintilie, G., Zhang, K., Su, Z., Li, S., Schmid, M.F., and Chiu, W. (2020). Measurement of atom resolvability in cryo-EM maps with Q-scores. Nat Methods *17*, 328-334. 10.1038/s41592-020-0731-1.

국 문 초 록

최근 나노디스크는 막단백질 연구에 많이 사용되고 있지만, 이 방법에 의한 막단백질의 안정화 메커니즘은 여전히 알려져 있지 않다. 이 연구는 EMPIAR에서 얻은 9개의 개별 초저온 전자 현미경 데이터를 3D variability로 분석하여 결과를 얻었고 이에 정량적 모델을 적용하여 나노 디스크 내의 다양한 막단백질의 분포를 종합적으로 분석했다.

분석 결과 나노디스크에 포함된 막단백질은 대부분 나노디스크의 가장자리로 이동하여 막 지지체 단백질과 접촉을 한다. 특히, 대장균 시토크롬 bd-I 산화효소의 막관통 나선 부분은 MSP와 직접적인 상호작용을 분명히 나타낸다. 또한 V-ATPase 구조에 대한 B-factor 분석을 통해 막단백질의 안정화가 MSP와의 직접적인 상호작용에 의해 유도된다는 것도 관찰하였다. 마지막으로 단백질 전체 평균 해상도의 차이는 크지 않았지만 MSP와의 직접적인 상호작용이 있는 막단백질 부분의 해상도가 향상되었음을 확인하였다. 종합적으로 우리의 연구는 나노디스크 내부의 막단백질이 MSP와의 상호작용에 의해 안정화된다는 것을 제안한다.

주요어 : 나노디스크, 막 지지체 단백질(MSP), 막단백질, 초저온 전자 현미경

학번 : 2020-24930